View metadata, citation and similar papers at core.ac.uk

brought to you by CORE

provided by Embry-Riddle Aeronautical University

Publications

2-14-2011

The Chromospheric Activity, Age, Metallicity, and Space Motions of 36 Wide Binaries

J. K. Zhao
Florida Institute of Technology

T. D. Oswalt
Florida Institute of Technology, oswaltt1@erau.edu

M. Rudkin
Florida Institute of Technology

G. Zhao
Chinese Academy of Sciences

Y. Q. Chen
Chinese Academy of Sciences

Follow this and additional works at: https://commons.erau.edu/publication

 Part of the Stars, Interstellar Medium and the Galaxy Commons

Scholarly Commons Citation

Zhao, J. K., Oswalt, T. D., Rudkin, M., Zhao, G., & Chen, Y. Q. (2011). The Chromospheric Activity, Age, Metallicity, and Space Motions of 36 Wide Binaries. *The Astronomical Journal, 141*(4). https://doi.org/10.1088/0004-6256/141/4/107

This Article is brought to you for free and open access by Scholarly Commons. It has been accepted for inclusion in Publications by an authorized administrator of Scholarly Commons. For more information, please contact commons@erau.edu.

The Astronomical Journal, 141:107 (11pp), 2011 April doi:10.1088/0004-6256/141/4/107
© 2011. The American Astronomical Society. All rights reserved. Printed in the U.S.A.

THE CHROMOSPHERIC ACTIVITY, AGE, METALLICITY, AND SPACE MOTIONS OF 36 WIDE BINARIES

J. K. Zhao[1,2], T. D. Oswalt[1], M. Rudkin[1], G. Zhao[2], and Y. Q. Chen[2]
[1] Florida Institute of Technology, Melbourne, FL 32901, USA; jzhao@fit.edu, toswalt@fit.edu, mrudkin@fit.edu
[2] Key Laboratory of Optical Astronomy, National Astronomical Observatories, Chinese Academy of Sciences, Beijing 100012, China; gzhao@bao.ac.cn, cyq@bao.ac.cn
Received 2010 August 25; accepted 2011 January 14; published 2011 February 14

ABSTRACT

We present the chromospheric activity (CA) levels, metallicities, and full space motions for 41 F, G, K, and M dwarf stars in 36 wide binary systems. Thirty-one of the binaries contain a white dwarf (WD) component. In such binaries, the total age can be estimated by adding the cooling age of the WD to an estimate of the progenitor's main-sequence lifetime. To better understand how CA correlates to stellar age, 14 cluster member stars were also observed. Our observations demonstrate for the first time that, in general, CA decays with age from 50 Myr to at least 8 Gyr for stars with $1.0 \leqslant V - I \leqslant 2.4$. However, little change occurs in the CA level for stars with $V - I < 1.0$ between 1 Gyr and 5 Gyr, consistent with the results of Pace et al. Our sample also exhibits a negative correlation between the stellar age and metallicity, a positive correlation between the stellar age and W space velocity component, and the W velocity dispersion increases with age. Finally, the population membership of these wide binaries is examined based upon their U, V, W kinematics, metallicity, and CA. We conclude that wide binaries are similar to field and cluster stars in these respects. More importantly, they span a much more continuous range in age and metallicity than is afforded by nearby clusters.

Key words: stars: activity – stars: late-type – white dwarfs

1. INTRODUCTION

Age is one of a star's properties that is the most difficult to determine. The Vogt–Russell theorem asserts that the structure of a star is uniquely determined by its mass and composition. Nucleosynthesis in the core results in changes in composition and this implies that at least some measurable property (properties) of a star must vary with age. Unfortunately, these changes are subtle and difficult to measure. It is ironic that the age of the universe (13.7 ± 0.2 Gyr; Bennett et al. 2003) is known to better precision than the age of any star other than the Sun. The present methods by which stellar ages can be estimated are seldom consistent within 50% (Soderblom 2010). Even the Sun does not reveal its age directly; this key calibration point is determined from the decay of radioisotope samples to be 4566^{+2}_{-1} Myr (Chaussidon 2007).

One of the "semifundamental" methods of stellar age determination is isochrone fitting the position of a star in the Hertzsprung–Russell (H-R) diagram. However, because of the degeneracy of theoretical isochrones, this technique does not work for the majority of stars—those on the lower main sequence (MS). Here small errors in luminosity or metallicity translate into large errors in age.

Ca II H&K features in the violet spectra of MS stars are one of the more well-studied indicators of chromospheric activity (CA). Early work by Wilson (1963, 1968) and Vaughan & Preston (1980) established Ca II H&K emission as a useful marker of CA in lower MS stars. In F to early M stars, Skumanich (1972) found that Ca II H&K emission, magnetic field strength, and rotation all decay as the inverse square root of stellar age.

Mamajek & Hillenbrand (2008) and others have shown that the CA versus age relation is much more complex than Skumanich envisioned; such factors as metallicity, photospheric contamination of CA indices, and variation in CA must be considered. Clusters provide only a limited range of ages and metallicities with which to investigate these effects.

A self-sustaining magnetic dynamo driven by rotation and convection is believed to be the source of CA in MS stars of spectral type F, G, K, and early M. According to this paradigm, due to magnetic breaking, rotational velocity decreases with age, which leads to a decrease in CA as well, unless angular momentum is sustained by tidal interaction as in the case of short-period binaries or maintained by convection as in late M type dwarfs.

Using a lower resolution analog of the Mount Wilson S index in eight clusters and the Sun, Barry et al. (1987) found that the decay of CA is well represented by an exponential over the age range from 10^7 to 6×10^9 yr. Barry (1988) adjusted the age of three clusters from Barry et al. (1987). Using a color correction $C'_{\rm cf}$ from Noyes et al. (1984), Barry empirically found that CA $\sim t^{1/e}$. In addition, he concluded that the star formation rate (SFR) in the solar neighborhood has not been constant, suggesting a recent burst of star formation because of a large number of stars in his youngest age bins. Working toward a more detailed understanding of the CA versus age relation, Soderblom et al. (1991) found that, while a power law is generally the best fit to the Ca II H&K versus age relation, it implies a constant SFR. Any different SFR causes the Skumanich relation to indicate an excess of young stars in the solar neighborhood. They also found that the calibrated cluster data presented in Barry et al. (1987) were consistent with a constant SFR.

Pace & Pasquini (2004) found that for several clusters older than 1 Gyr there appeared to be a constant activity level. Pace et al. (2009) believed stars change from active to inactive, crossing the activity range corresponding to the so-called Vaughan–Preston gap, on a timescale that might be as short as 200 Myr. If true, this would bring into question whether the Skumanich relation is valid for MS stars in all age regimes.

Among wide white dwarf WD+dM binaries Silvestri et al. (2005) used the cooling ages of white dwarf (WD) components, plus an average estimate for MS lifetime, to explore the activity versus age relation among lower MS stars. This study confirmed that stars later than spectral type dM3 do not exhibit a Skumanich-style CA versus age relation. In a study of activity among unresolved WD+dM cataclysmic variable candidates, Silvestri et al. (2006) used the WD cooling times alone as a

lower age limit. Both of these studies found the general trend seen in clusters, i.e., that later dM spectral types remain active at a roughly constant level for a longer period of time than earlier dM spectral types, whereupon each star becomes inactive. The transition from active to inactive appears to take place over a relatively short period of time. However, in both studies some dM stars in binaries were found to exhibit activity more characteristic of brighter, bluer, and more massive M dwarfs than seen in clusters. West et al. (2008) examined the age–activity relation among a sample of over 38,000 low-mass (M0–M7) stars drawn from the Sloan Digital Sky Survey (SDSS) Data Release 5 and also found that later spectral types remain active longer. It is important to note that late-type stars do not seem to decline in activity monotonically; they are either "on" if young, or "off" if old. While the activity turnoff point on the lower MS constrains a cluster's age it is not a useful means for estimating the age of a field star.

This paper describes our analysis of a sample of common proper motion binary (CPMB) systems. Most of the systems selected have a late MS star paired with a WD component. All have relatively wide orbital separations ($\langle a \rangle \sim 10^3$ AU; Oswalt et al. 1993). Thus, each component is assumed to have evolved independently, unaffected by mass exchange or tidal coupling that complicates the evolution of closer pairs (Greenstein 1986). It is also assumed that members of such binaries are coeval. Essentially, each may be regarded as an open cluster with only two components. Such binaries are far more numerous than clusters and span a much broader and more continuous range in age. Thus, they are potentially very valuable to investigations of phenomena that depend upon age. The total age of a CPMB can be estimated from the cooling age of the WD component added to an estimate of its progenitor's MS lifetime. Since some CPMBs in our sample have ages well beyond the present ∼4 Gyr nearby cluster limit, this provides an opportunity to test the CA versus age relation in much older MS stars.

Wide binaries present another opportunity. The metallicity can be measured from the spectra of the MS components. Presumably this is also the original metallicity of the WD progenitor. In addition, the radial velocities of the MS stars are easy to determine. Since proper motions are available, with trigonometric or photometric parallaxes, full space motions for all systems in the observed sample can be estimated. Thus, CPMBs present an opportunity to investigate the relations among age, metallicity, and space motion, as well as population membership even for WDs, which often have weak or no spectral features.

In Section 2, we present an overview of the observations and reductions for our sample. A discussion of the CA versus age relation is given in Section 3. Our age and metallicity relation is presented in Section 4. In Section 5, we describe our analysis of population membership. We conclude with a discussion of the implications of our findings in Section 6.

2. OBSERVATIONS AND DATA REDUCTION

Most stars chosen for this study are components of wide MS+WD pairs from the Luyten (1979) and Giclas et al. (1971) proper motion catalogs chosen by Oswalt et al. (1988). A key impetus for using such pairs in this study is that the total lifetime of each pair should be approximately the age derived from measurements of the MS component. In addition, the total age of a pair should be approximately the sum of the WD component's cooling time and the MS lifetime of its progenitor.

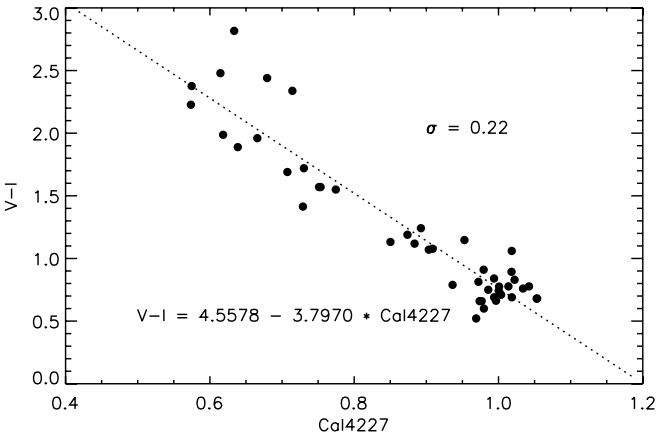

Figure 1. Relation between $V - I$ and the flux ratio of CaI4227. The dotted line is a least-squares fit. We used this relation to estimate the $V - I$ color for a few stars whose photometric data were unavailable. See the text for details.

Table 1 gives the observed data for 36 wide binaries. Column 1 is a unique ID number. Columns 2–4 list each component's name, right ascension, and declination (coordinates are for epoch 1950). The V magnitudes and original low-resolution spectroscopic identifications are given in Columns 5–8. Column 9 is the observation date for the high-resolution (∼2 Å) spectra in the present study. Columns 10–13 list the proper motion, direction of proper motion (measured east of north), position angle (centered on the primary measured east of north), and separation of the components (in arcseconds), respectively. Of the 36 wide binaries, five systems consist of two MS stars, one system is a triple WD+dK+dM, and the remaining 30 are MS+WD pairs.

A sample of cluster MS stars of known age, such as IC 2391, IC 2602, and M67, previously studied by Patten & Simon (1993, 1996), Barrado y Navascués et al. (2004), and Giampapa et al. (2006), were adopted as "CA standards." These stars were routinely observed in the course of our observing program for the CPMBs. Table 2 provides the observational information for these cluster member stars. Column 1 is a unique ID. Columns 2–4 list the name, V magnitude, and observation date. The colors $V - I$ and $B - V$ are given in Columns 5 and 6. The CA flux ratio $S_{\rm HK}$ (see Section 3.1), age, and cluster membership are given in Columns 7–9. The last column provides the corresponding literature source for each star.

2.1. BVRI Photometry

We used BVRI photometric data for our wide binaries from Smith (1997) whenever available. Photometric data for some stars that were not in this source were taken from the literature identified by the Simbad Astronomical Database (Genova 2006). Photometric colors of other stars were estimated from our spectra by empirical calibrations. For example, Figure 1 is the relation between the $V - I$ and CaI4227 flux ratio. The feature of this index is within 4211–4242 Å and the continuum ranges within 4152–4182 Å. The filled circles are stars with known $V - I$ color. The dotted line is a least-squares fit. The scatter $\sigma_{\rm V-I} \approx 0.22$. We used this relation to estimate the $V - I$ for stars with no published colors. For the stars in clusters IC 2602, IC 2391, and M67, photometric colors were taken from Barnes et al. (1999, and references therein), Patten & Simon (1996), and Giampapa et al. (2006).

Table 1
Observed Wide Binaries

ID	Name (Star 1/Star 2)	R.A. (B1950.0)	Decl. (B1950.0)	M_1	Sp1[a]	M_2	Sp2[a]	UT (mm/yy)	μ (arcsec yr^{-1})	θ_μ (deg)	pos (deg)	Sep (arcsec)	Location
(1)	(2)	(3)	(4)	(5)	(6)	(7)	(8)	(9)	(10)	(11)	(12)	(13)	
1	CD-31 1454/LP888-25	03 32 36	−31 14 00	11.8	dG	15.9	dK	02/05	0.51	186	264	223	CTIO
2	G114-B8A/B	08 58 17	−04 10 24	11.0	dK0	15.9	dG2	02/05	0.10	150	151	54	CTIO
3	BD+12 937/G102-39	05 51 05	12 23 48	7.6	dF8	15.7	DC	02/04	0.28	184	47	91	CTIO
4	G272-B5A/B	02 00 31	−17 07 30	12.5	dG	15.8	DA	02/05	0.05	181	79	72	CTIO
5	BD−03 2935/LP670-9	10 27 24	−03 57 00	11.2	dG	18.7		02/05	0.18	103	139	35	CTIO
6	G163-B9A/B	10 43 39	−03 24 06	12.6	dF9	15.6		02/05	0.08	115	122	76	CTIO
7	BD+23 2539/LP378-537	13 04 48	22 43 00	9.8	dK0	16.2	DA	02/04	0.11	300	106	20	CTIO
8	CD-25 8487/LP849-59	11 07 00	−25 43 00	9.3	sdM0	16.8	DC	02/04	0.25	106	181	100	CTIO
9	CD-28 3361/LP895-41	06 42 34	−28 30 48	11.2	dK	16.8	DA	02/04	0.16	227	75	16	CTIO
10	BD−5 3450/LP674-29	12 09 48	−06 05 00	12.0	dK5	17.2	DC	02/05	0.44	220	102	202	CTIO
11	BD−18 2482/LP786-6	08 45 18	−18 48 00	12.8	dK3	15.1	DB	02/04	0.16	268	236	31	CTIO
12	40 Eri A/B/C	04 13 03	−07 44 06	5.3	dG	9.5	DA	02/04, 02/05	4.08	213	105	82	CTIO
13	CD-31 7352/LP902-30	09 28 20	−31 53 12	9.3	dK	14.5	dM	02/05	0.34	348	206	12	CTIO
14	LP684-1/2	15 54 00	−04 41 00	12.7	dM	15.5	dM	02/05	0.32	244	202	5	CTIO
15	BD−18 3019/LP791-55	10 43 30	−18 50 00	12.9	dM0	16.6	DQ	02/04	1.98	250	356	7.5	CTIO
16	LP856-54/53	13 48 30	−27 19 00	13.9	dM	15.1	DA	02/04	0.24	166	233	9	CTIO
17	LP498-25/26	13 36 45	12 23 48	13.9	dM	14.5	DB	02/04	0.19	134	307	87	CTIO
18	LP672-2/1	11 05 30	−04 53 00	12.6	dM6	13.8	DA	02/04	0.44	184	160	279	CTIO
19	LP916-26/27	15 42 18	−27 30 00	15.5	dM	16.3	DB	02/04	0.24	235	330	52	CTIO
20	LP891-13/12	04 43 18	−27 32 00	15.6	dM	15.9	DQ	02/05	0.24	246	62	49	CTIO
21	LP783-2/3	07 38 02	−17 17 24	12.9	dM	17.6	DB	02/04, 02/05	1.26	117	276	21	CTIO
22	CD-37 10500/L481-60	15 44 12	−37 46 00	6.8	dG	13.2	DA	02/05	0.48	243	131	15	CTIO
23	CD-59 1275/L182-61	06 15 36	−59 11 24	7.0	dG0	13.7	DB	02/04, 02/05	0.33	190	302	41	CTIO
24	LP888-63/64	03 26 45	−27 18 36	13.9		15.6		02/05	0.83	63	227	7	CTIO
25	CD-38 10983/10980	16 20 38	−39 04 42	6.1	dG	10.7	DA	02/04, 02/05	0.08	95	248	345	CTIO
26	LHS193A/B	04 30 50	−39 08 55	11.7	dM	17.7	DB	02/05	1.023	44.5			CTIO
27	LHS300A/B	11 08 58	−40 49 05	13.2	dK	17.8	DB	02/05	1.277	264.5			CTIO
28	LP387-2/1	16 44 18	24 06 00	16.8	dG	17.6	DG	07/05	0.11	163	296	37	KPNO
29	BD−8 0980/G156-64	22 53 12	−08 05 24	9.0	dG	16.4	DA	07/05	0.59	91	168	43	KPNO
30	G171-62/G172-4	00 30 17	44 27 18	10.3	dK	16.6	DA	11/06	0.16	285.9			KPNO
31	BD−1 469/LP592-80	03 15 48	−01 06 18	6.6	dG	17.2	DA	11/06	0.18	192	50	49	KPNO
32	G216-B14A/B	22 58 49	40 40 12	12.0		15.5		11/06	0.07	215	261	23	KPNO
33	BD+44 1847/G116-16	09 11 51	44 15 36	10.2		15.5		11/06	0.28	174	95	1020	KPNO
34	G273-B1A/B	23 50 54	−08 21 06	12.0	dG	16.4	DA	11/06	0.12	75	210	36	KPNO
35	G95-B5A/B	02 20 44	22 14 00	9.2		15.6		11/06	0.15	113	94	26	KPNO
36	BD+26 730/LP358-525	04 33 42	27 02 00	9.4	dK	16.3	DA	11/06	0.28	122	338	128	KPNO

Notes. Units of right ascension are hours, minutes, and seconds, and units of declination are degrees, arcminutes, and arcseconds. Magnitude values (except 26 and 27) are m_{pg} magnitudes from Oswalt et al. (1988).

[a] Spectral types for the WD and MS stars were determined from low-resolution (∼7–15 Å) spectra (Oswalt et al. 1988, 1991, 1993).

2.2. Spectroscopic Observations

In the southern hemisphere, observations were conducted at Cerro Tololo Inter-American Observatory (CTIO) using the Blanco 4 m telescope. The Ritchey–Chrétien (R-C) Cassegrain spectrograph was used on two separate observing runs (2004 February and 2005 February) to obtain optical spectroscopy of CPMBs, as well as the CA standard stars. During the two observation runs, the KPGL1 grating was used to obtain spectra with a scale of 0.95 Å pixel^{-1}. A Loral 3K CCD (L3K) was used with the R-C spectrograph. It is a thinned 3K × 1K CCD with 15 μm pixels. A spectral range of approximately 3800–6700 Å was achieved.

Northern hemisphere observations were conducted at Kitt Peak National Observatory (KPNO) using the Mayall 4 m telescope. The R-C spectrograph, with the BL450 grating set for the second order to yield a resolution of 0.70 Å pixel^{-1}, was used to obtain optical spectra during the 2005 July and 2006 November observing runs. The 2K × 2K T2KB CCD camera with 24 μm pixels was used to image the spectra. An 8 mm $CuSO_4$ order-blocking filter was added to decrease first-order overlap at the blue end of the spectrum. A spectral range of approximately 3800–5100 Å was achieved.

2.3. Data Reduction

The data were reduced with standard IRAF[3] reduction procedures. In all cases, program objects were reduced with calibration data (bias, flat, arc, flux standard) taken on the same night. Data were bias-subtracted and flat-fielded, and one-dimensional spectra were extracted using the standard aperture extraction method. A wavelength scale was determined for each spectrum using HeNeAr arc lamp calibrations. Flux standard stars were used to place the spectra on a calibrated flux scale. We emphasize that these are only relative fluxes, as most nights were not spectrophotometric.

[3] IRAF is distributed by the National Optical Astronomy Observatory, which is operated by the Association of Universities for Research in Astronomy, Inc., under cooperative agreement with the National Science Foundation (http://iraf.noao.edu).

Table 2
Cluster Member Stars Observed

ID (1)	Name (2)	V (3)	UT (4)	$V-I$ (5)	$B-V$ (6)	S_{HK} (7)	Age (Gyr) (8)	Cluster (9)	Ref[a] (10)
37	[RSP95] 15	11.75	02/05	1.0600	0.9300	0.6819	$0.050^{0.055}_{0.045}$	IC2602	1
38	[RSP95] 32	15.06	02/05	2.1600	1.6300	1.5799	$0.050^{0.055}_{0.045}$	IC2602	1
39	[RSP95] 66	11.07	02/04	0.8300	0.6800	0.4241	$0.050^{0.055}_{0.045}$	IC2602	1
40	[RSP95] 70	10.92	02/04	0.7100	0.6900	0.3553	$0.050^{0.055}_{0.045}$	IC2602	1
41	[RSP95] 72	10.89	02/05	0.7600	0.6400	0.5110	$0.050^{0.055}_{0.045}$	IC2602	1
42	[RSP95] 80	11.75	02/04	1.0900	0.9300	0.5738	$0.050^{0.055}_{0.045}$	IC2602	1
43	VXR PSPC 12	11.86	02/04	0.9100	0.8300	0.5429	$0.050^{0.055}_{0.045}$	IC2391	2
44	VXR PSPC 14	10.45	02/04	0.6900	0.5700	0.4302	$0.050^{0.055}_{0.045}$	IC2391	2
45	VXR PSPC 70	10.85	02/04	0.7500	0.6400	0.3716	$0.050^{0.055}_{0.045}$	IC2391	2
46	VXR PSPC 72	11.46	02/04	0.8400	0.7300	0.4984	$0.050^{0.055}_{0.045}$	IC2391	2
47	VXR PSPC 76a	12.76	02/04	1.2414	1.0400	0.8793	$0.050^{0.055}_{0.045}$	IC2391	2
48	VXR PSPC 77a	9.91	02/04	0.6000	0.5000	0.4184	$0.050^{0.055}_{0.045}$	IC2391	2
49	Cl* NGC 2682 SAND 785	14.8	02/05	0.8315	0.6500	0.3233	$4.000^{4.300}_{3.800}$	M67	3
50	Cl* NGC 2682 SAND 1477	14.6	02/05	0.8497	0.6700	0.2981	$4.000^{4.300}_{3.800}$	M67	3

Note. [a] (1) Barnes et al. 1999; (2) Patten & Simon 1996; (3) Giampapa et al. 2006.

The radial velocity of each MS star was determined by cross-correlation between the observed spectra and a set of MS template spectra. The F, G, and K template spectra were generated from a theoretical atmosphere grid (Castelli & Kurucz 2003). The dM template spectra were compiled using observed M dwarf spectra from the SDSS[4]. The wavelength ranged from roughly 3900–9200 Å (see Bochanski et al. 2007). Our typical internal measurement uncertainties in radial velocity were $\sigma_{v_r} = \pm$ 4.6 km s^{-1}. The final radial velocities listed in Column 5 of Table 3 were corrected to the heliocentric frame.

3. CA–AGE RELATION

3.1. Measurement of S_{HK}

The flux ratio

$$S_{HK} = \alpha \frac{H+K}{R+V} \quad (1)$$

was determined for each MS star, where H and K are the fluxes measured in 2 Å rectangular windows centered on the line cores of Ca II H&K. Here R and V are the fluxes measured in 20 Å rectangular "pseudocontinuum" windows on either side. Although these are not strictly equivalent to the triangular windows Wilson (1968) used with his photomultiplier-based spectrometer, Hall et al. (2007) have shown that using 1.0 Å rectangular H&K windows produces results that are easily calibrated to the Baliunas et al. (1995) analysis of Wilson's (1968) original survey of bright MS stars. Our choice of 2 Å windows is set by the resolution of the CTIO and KPNO instrumentation, but it detects Ca II H&K emission nearly as well and allows fainter stars to be observed. Gray et al. (2003) have shown that even a resolution of ∼4 Å can produce useful measures of S_{HK}. In our measurements, the scale α is 10.0, reflecting the fact that the continuum windows are 10 times wider than the H&K windows.

In our sample some stars were observed two or three times. In such cases, the mean of these measurements was adopted as the star's S_{HK} and the scatter as the uncertainty. For those stars observed only once, we adopted the average uncertainty derived from those stars having more than one observation (±4.6%). The S_{HK} indices of all the MS stars are shown in Column 4 of Table 3. For the purpose of this study, we need only a calibration of CA versus age on our instrumental system. Some stars were observed both at CTIO and KPNO. We found an empirical calibration: $S_{ctio} = S_{kpno}$+0.095. To remove this small instrumental effect, all the S_{HK} measured at KPNO were transformed into the CTIO instrumental system with this relation.

3.2. The Age Determination

Our sample includes 14 cluster member stars: six in IC2602, six in IC2391, and two in M67. The ages of IC2602 and IC 2391 are approximately the same (∼50 ± 5 Myr; Barrado y Navascués et al. 2004). They obtained intermediate-resolution optical spectroscopy of 44 potentially very low mass members of IC2391 and derived the cluster age from a comparison of several theoretical models. The most recent age determination for M67 is 4.05 ± 0.05 Gyr (Jorgensen & Lindegren 2005).

Among our 31 systems containing WD components, the ages of 23 were determined by using computed cooling times of WD companions added to estimates of their progenitor's MS lifetimes. The T_{eff} and log g of each WD companion were obtained from the literature (see Table 4). The ages of the remaining eight wide binaries were not obtained because the T_{eff} and log g of WD companions could not be obtained from our spectra (three: DC type; one: DQ; four: low signal-to-noise ratio) and could not be found in the literature. In cases where uncertainties were not given, we adopted 200 K and 0.05 as the average uncertainty for T_{eff} and log g, respectively. This decision was based on the recommendation of Bergeron et al. (1992) who believe the internal errors are typically 100–300 K in T_{eff} and 0.02–0.06 in log g. From the T_{eff} and log g of each WD, its mass (M_{WD}) and cooling time (t_{cool}) were estimated from Bergeron's cooling sequences[5]. For the pure hydrogen model atmospheres above T_{eff} = 30,000 K, we used the carbon-core cooling

[4] http://www.astro.washington.edu/slh/templates

[5] The cooling sequences can be downloaded from the Web site http://www.astro.umontreal.ca/∼bergeron/CoolingModels/.

Table 3
Main Sequence Components of the Wide Binary Sample

ID	$V-I$	$B-V$	S_{HK}	v_r (km s^{-1})	π (mas)	U (km s^{-1})	V (km s^{-1})	W (km s^{-1})	[Fe/H]	Age (Gyr)
(1)	(2)	(3)	(4)	(5)	(6)	(7)	(8)	(9)	(10)	(11)
1a	0.5210	0.8230	0.2303	76.1 ± 7.3	5.89 ± 2.77	−329.0	−242.5	−101.4	−0.48 ± 0.02	
2a	0.6595	0.5660	0.2843	16.1 ± 4.3	9.06 ± 2.68	−42.5	−38.6	11.7	−0.17 ± 0.07	
2b	1.0701	0.9111	0.2413	114.3 ± 2.1	9.06 ± 2.68	10.3	−109.3	54.9	−0.40 ± 0.08	
3	0.6624	0.5699	0.2891	58.8 ± 9.7	18.70 ± 0.80	26.4	−65.8	−39.0	−0.25 ± 0.02	
4	0.6800	0.5230	0.2689	28.3 ± 5.4	62.95	−10.3	16.5	−19.1	−0.34 ± 0.06	
5	0.6901	0.6762	0.2666	−54.3 ± 6.1	28.3	−51.2	44.0	−18.6	0.10 ± 0.01	
6	0.7420	0.5970	0.4582	−20.8 ± 6.9	83.3	−18.5	18.6	−7.1	−0.25 ± 0.15	
7	0.7754	0.6422	0.3150	−7.7 ± 4.5	56.7	0.4	4.4	0.4	0.06 ± 0.04	$1.0^{1.2}_{0.9}$
8	0.7892	0.6963	0.2856	28.5 ± 4.9	26.76±1.09	−59.4	−8.6	30.9	−0.16 ± 0.06	
9	1.0776	0.9720	0.3454	27.0 ± 1.6	28.17±0.06	−6.4	−15.4	−26.4	−0.13 ± 0.13	
10	1.1181	0.9884	0.3180	55.9 ± 1.6	22.94±1.63	−0.3	−101.2	5.9	−0.48 ± 0.02	
11	1.1316	1.0362	0.4074	69.2 ± 5.6	29.49	35.6	−53.3	3.5	0.19 ± 0.09	$2.0^{2.8}_{1.4}$
12a	1.1469	0.7750	0.3051	−37.9 ± 1.7	198.25 ± 0.84	−104.0	−8.5	−37.4	−0.17 ± 0.17	$5.0^{6.1}_{4.0}$
12c	2.8297	1.3938	3.0759	−54.0 ± 1.7	198.25 ± 0.84	−104.0	−8.5	−37.4	−0.17 ± 0.17	$5.0^{6.1}_{4.0}$
13a	1.1891	0.9822	0.3140	21.8 ± 2.0	51.71 ± 0.91	19.6	−9.4	28.7	−0.30 ± 0.10	
13b	2.3761	1.4432	0.5585	33.8 ± 3.1	51.71 ± 0.91	21.6	−21.6	31.7	−0.22 ± 0.08	
14a	1.4140	1.2120	0.4563	67.2 ± 1.8	42.69	−58.5	−23.0	58.5	0.19 ± 0.09	
14b	2.2270	0.6870	0.5730	60.3 ± 6.9	42.69	−52.8	−23.5	54.5	0.05 ± 0.09	
15	1.8888	1.4484	0.6202	57.7 ± 2.0	56.92	236.9	−187.8	−229.5	−0.25 ± 0.15	$3.6^{5.0}_{2.7}$
16	1.9870	1.4550	0.74958	14.4 ± 4.2	49.63	−28.6	−11.1	−4.2	0.15 ± 0.05	$1.2^{1.4}_{0.9}$
17	2.3380	1.5710	1.0492	11.7 ± 5.2	46.12	−33.3	3.1	11.8	−0.24 ± 0.10	$1.5^{2.9}_{0.8}$
18	2.4790	1.5020	0.7738	28.6 ± 4.2	57.70 ± 14.40	−22.9	−39.0	8.8	−0.02 ± 0.03	$3.5^{4.5}_{2.5}$
19	2.8165	1.6318	0.9172	−53.4 ± 4.0	40.05	48.1	−9.6	−7.5		$2.2^{4.8}_{1.6}$
20	2.8474	1.5111	2.5424	24.0 ± 3.2	38.80	−14.0	3.4	−33.0		
21	4.2570	1.8760	1.0893	−24.6 ± 3.9	102.00 ± 14.00	−65.8	−3.1	40.6		$2.4^{4.2}_{1.8}$
22	0.8933	0.7180	0.3031	−18.3 ± 10.1	65.1 ± 0.4	24.8	−24.1	15.5	0.02 ± 0.08	$1.1^{1.3}_{0.9}$
23	0.7769	0.5900	0.27162	−41.9 ± 4.2	27.5 ± 0.5	−63.3	12.9	−17.8	0.03 ± 0.07	$1.4^{2.4}_{0.4}$
24	1.8366	1.5000	1.2597	3.2 ± 3.8	57.6	29.6	−4.0	83.1		$3.6^{5.6}_{2.2}$
25	0.8133	0.630	0.32504	−2.5 ± 4.1	77.69 ± 0.86	−9.5	9.7	2.1	−0.10 ± 0.12	$1.4^{2.3}_{0.9}$
26	1.5700	1.1600	0.3815	56.6 ± 4.4	32.06 ± 1.65	131.7	−50.6	48.2	−0.45 ± 0.26	$7.5^{8.7}_{6.1}$
27	1.6900		0.3835	145.0 ± 1.8	32.3	100.3	−195.3	−46.3	−0.95 ± 0.25	$7.9^{9.0}_{5.5}$
28a	1.0215	0.8394	0.2264	−29.9 ± 2.2	45.0	−14.0	−19.3	27.4	0.04 ± 0.06	
28b	0.901	0.8470	0.2054	−32.1 ± 5.8	45.0	−14.2	−20.4	29.3	0.03 ± 0.07	
29	0.7100	0.5300	0.2189	−28.1 ± 4.1	28.7 ± 1.3	80.4	−38.6	−12.3	−0.40 ± 0.02	$3.5^{3.9}_{3.0}$
30	0.8800	0.9800	0.2389	44.4 ± 1.5	9.52 ± 1.63	101.3	−20.3	−36.3	−0.23 ± 0.03	$1.6^{2.4}_{1.0}$
31	0.3758[a]	1.0400	0.1585	33.2 ± 1.9	14.68 ± 0.96	−19.7	−29.4	−49.3	−0.16 ± 0.04	$2.6^{3.9}_{1.3}$
32	2.0889[a]		1.0034	1.6 ± 1.2					−0.15 ± 0.05	$1.2^{1.3}_{1.0}$
33	0.7160	0.6600	0.1820	−61.4 ± 12.0	19.36 ± 1.30	−57.6	−65.3	−27.8	−0.40 ± 0.10	$1.6^{1.8}_{1.4}$
34	0.6861[a]		0.2081	28.9 ± 1.4					−0.16 ± 0.06	$3.4^{4.2}_{2.7}$
35	0.9195[a]		0.3607	27.3 ± 3.6	21.65	26.4	−11.3	−7.7	−0.50 ± 0.03	$3.4^{4.2}_{2.6}$
36	1.52	1.1200	1.7876	42.7 ± 1.3	56.02 ± 1.21	35.8	−11.6	4.4	−0.21 ± 0.03	$4.5^{5.4}_{3.6}$

Note. [a] $V-I$ is from the relation in Figure 1.

models of Wood (1995), with thick hydrogen layers of $q_H = M_H/M_* = 10^{-4}$. For T_{eff} below 30,000 K, we used cooling models similar to those described in Fontaine et al. (2001) but with carbon–oxygen cores and $q_H = 10^{-4}$ (see Bergeron et al. 2001). For the pure helium model atmospheres, we used similar models but with $q_H = 10^{-10}$. M_{WD} and t_{cool} were then calculated by spline interpolation based on T_{eff} and log g. In Table 4, Columns 6 and 7 list the final M_{WD} and t_{cool} for these 23 WDs. Although T_{eff} and log g are from different literature sources, the parameters are consistent for common stars in these references. Thus, there appears to be no systematic uncertainties expected between T_{eff} and log g we used.

Using the initial–final mass relation (IFMR; Equations (2) and (3) presented in Catalán et al. 2008a), we then estimated the progenitor masses M_i of the WDs. There are two WDs whose masses are lower than 0.5 $M_\odot$, and the current IFMR does not extend to such low-mass objects. From Figure 2 in Catalán et al. (2008a), we adopted $M_i \sim 1.25\,M_\odot$ for $M_{WD} < 0.5\,M_\odot$. Next, using the third-order polynomial of Iben & Laughlin (1989),

Table 4
White Dwarf Components of the Wide Binary Sample

ID	Name	Sp	$T_{\rm eff}$ (K)	log g	$M_{\rm WD}$ ($M_\odot$)	Cooling Time (Gyr)	$M_{\rm i}$ ($M_\odot$)	$t_{\rm evol}$ (Gyr)	Ref[a]
(1)	(2)	(3)	(4)	(5)	(6)	(7)	(8)	(9)	(10)
7b	LP378-537	DA	10800 ± 120	8.21 ± 0.05	0.732 ± 0.032	0.6760 ± 0.0626	3.02 ± 0.23	$0.3^{0.5}_{0.2}$	1
11b	LP786-6	DB	17566 ± 200	7.97 ± 0.05	0.579 ± 0.028	0.1182 ± 0.0135	1.56 ± 0.29	$1.9^{2.7}_{1.3}$	2
12b	40Eri B	DA	16570 ± 350	7.86 ± 0.05	0.540 ± 0.019	0.1122 ± 0.0116	1.15 ± 0.20	$4.9^{6.0}_{3.9}$	4
15b	LP791-55	DQ	6190 ± 200	8.09 ± 0.05	0.630 ± 0.029	2.8244 ± 0.6080	2.09 ± 0.31	$0.8^{2.1}_{0.3}$	3
16b	LP856-53	DA	10080 ± 200	8.17 ± 0.05	0.705 ± 0.032	0.7572 ± 0.0911	2.82 ± 0.23	$0.4^{0.6}_{0.2}$	4
17b	LP498-26	DB	16779 ± 200	8.00 ± 0.05	0.595 ± 0.027	0.1475 ± 0.0155	1.73 ± 0.28	$1.4^{2.7}_{0.6}$	2
18b	LP672-1	DA	15996 ± 11	7.753 ± 0.002	0.486 ± 0.001	0.1066 ± 0.0004	1.25 ± 0.01	$3.4^{4.4}_{2.4}$	5
19b	LP916-27	DB	10826 ± 200	8.00 ± 0.05	0.585 ± 0.029	0.5365 ± 0.0531	1.62 ± 0.30	$1.7^{4.3}_{1.2}$	2
21b	LP783-3	DZ	7590 ± 200	8.07 ± 0.05	0.619 ± 0.031	1.4854 ± 0.1856	1.93 ± 0.31	$0.9^{2.7}_{0.3}$	3
22b	L481-60	DA	10613 ± 18	8.12 ± 0.03	0.675 ± 0.018	0.6167 ± 0.0254	2.56 ± 0.19	$0.5^{0.7}_{0.3}$	6
23b	L182-61	DB	16714 ± 200	8.07 ± 0.05	0.605 ± 0.029	0.1539 ± 0.0160	1.83 ± 0.30	$1.2^{2.2}_{0.4}$	2
24b	LP888-63	DA	9408 ± 8	7.93 ± 0.02	0.559 ± 0.011	0.6515 ± 0.0159	1.35 ± 0.11	$3.0^{5.0}_{1.6}$	3
25b	CD-38 10980	DA	24276 ± 200	8.01 ± 0.05	0.641 ± 0.028	0.0279 ± 0.0043	2.21 ± 0.29	$0.7^{1.6}_{0.3}$	6
26b	LHS193B	DA	4394 ± 200	8.10 ± 0.05	0.632 ± 0.032	6.6900 ± 0.8100	2.11 ± 0.33	$0.8^{1.3}_{0.3}$	7
27b	LHS300B	DA	4705 ± 200	7.80 ± 0.05	0.456 ± 0.026	4.5385 ± 0.7298	1.25 ± 0.01	$3.4^{4.4}_{2.4}$	7
29b	G156-64	DA	7165 ± 165	8.43 ± 0.07	0.869 ± 0.046	3.2983 ± 0.4292	4.02 ± 0.34	$0.1^{0.3}_{0.1}$	4
30b	G172-4	DA	10440 ± 240	8.02 ± 0.07	0.613 ± 0.043	0.5566 ± 0.0803	1.92 ± 0.45	$1.1^{1.9}_{0.3}$	8
31b	LP592-80	DA	7520 ± 260	8.01 ± 0.45	0.600 ± 0.256	1.2822 ± 0.7289	1.78 ± 0.20	$1.3^{2.0}_{0.3}$	1
32b	G216-B14B	DA	9860 ± 226	8.20 ± 0.07	0.724 ± 0.045	0.8443 ± 0.1246	2.96 ± 0.33	$0.3^{0.4}_{0.2}$	4
33b	G116-16	DA	8750 ± 201	8.29 ± 0.07	0.780 ± 0.045	1.3397 ± 0.1785	3.37 ± 0.33	$0.2^{0.3}_{0.1}$	4
34b	G273-B1B	DA	18529 ± 37	7.79 ± 0.01	0.509 ± 0.004	0.0617 ± 0.0136	0.83 ± 0.04	$3.4^{4.0}_{2.7}$	5
35b	G94-B5B	DA	15630 ± 65	7.89 ± 0.01	0.555 ± 0.005	0.1456 ± 0.0384	1.31 ± 0.05	$3.3^{4.0}_{2.4}$	5
36b	LP358-525	DA	5620 ± 110	8.14 ± 0.07	0.673 ± 0.044	4.0693 ± 0.8147	2.54 ± 0.46	$0.5^{0.8}_{0.2}$	4

Notes. [a] This column lists the source of $T_{\rm eff}$, log g. (1) Catalán et al. 2008b; (2) Voss et al. 2007; (3) Sion et al. 2009; (4) Bergeron et al. 1995; (5) Koester et al. 2009; (6) Koester et al. 2001; (7) Monteiro et al. 2006; (8) Weidemann & Koester 1984.

$$\log t_{\rm evol} = 9.921 - 3.6648(\log M_{\rm i}) + 1.9697(\log M_{\rm i})^2 - 0.9369(\log M_{\rm i})^3, \quad (2)$$

we determined the MS lifetime $t_{\rm evol}$ (in years) corresponding to each $M_{\rm i}$, progenitor mass of the WD (in $M_\odot$). Columns 8 and 9 in Table 4 are $M_{\rm i}$ and $t_{\rm evol}$ we derived for 23 WDs. Finally, the total ages of these wide binaries were computed by adding $t_{\rm evol}$ to the cooling ages of the WDs ($t_{\rm cool}$; Column 11 in Table 3).

Independent age determinations for four pairs were found in the literature. These pairs are listed in Table 5. Column 1 gives their identifications. Columns 2 and 3 list the ages included in Holmberg et al. (2009) and Valenti & Fischer (2005), respectively. It can be seen that our ages are younger than isochrone fitting ages in all four cases. For 40 Eri A the isochrone fitting age is unreasonably large, while our age of this star is consistent with the rotation age 4.75 ± 0.75 Gyr from Barnes (2007). For CD-37 10500, the error bar is too large for isochrone fitting age to be useful. It is very difficult to estimate the age for K and M dwarfs with the isochrone fitting method because of the narrow vertical dispersion of isochrones within the MS in an H-R diagram. Small uncertainties in luminosity and metallicity cause large uncertainties in age. Using the WD cooling times plus the estimated progenitor lifetimes should give a more consistent age for such stars. Note that the internal uncertainties of our age determinations are smaller than those derived from isochrone fitting.

Although we have taken a similar approach, there are a few differences between our age determinations and those by Silvestri et al. (2005) and Silvestri et al. (2006). Silvestri et al. (2006) only used the WD cooling time as a lower limit to the age of each binary without considering the WD progenitor's lifetime in evaluating the age–activity relation among close binaries. Therefore, the ages were somewhat less than actual ages. In Silvestri et al. (2005), each age was estimated from the WD's cooling time plus an estimate of its progenitor's lifetime. The $M_{\rm i}$ of each WD was computed from the IFMR of Weidemann (2000) using an adopted mean WD mass of 0.61 $M_\odot$. We explicitly computed $M_{\rm i}$ of each WD from the IFMR of Catalán et al. (2008a) using our own estimate of its current mass ($M_{\rm f}$). In view of this, our method should provide more precise age estimates.

Table 5
Comparison between Our Ages and Those from the Literature

Name	Age$_{\rm n}$[a] (Gyr)	Age$_{\rm v}$[b] (Gyr)	Age (Gyr)
(1)	(2)	(3)	(4)
40 Eri A	∼	$12.2^{14.5}_{8.5}$	$5.0^{6.1}_{4.0}$
CD-38 10983	$2.5^{7.0}_{\sim}$	$2.0^{3.9}_{0.4}$	$1.2^{2.2}_{0.4}$
CD-59 1275	$5.9^{6.6}_{5.4}$	$3.7^{4.7}_{3.4}$	$1.4^{2.4}_{0.4}$
CD-37 10500	$7.4^{13.0}_{1.9}$	$4.4^{7.0}_{1.4}$	$1.1^{1.3}_{0.9}$

Notes.
[a] Ages are from Holmberg et al. (2009).
[b] Ages are from Valenti & Fischer (2005).

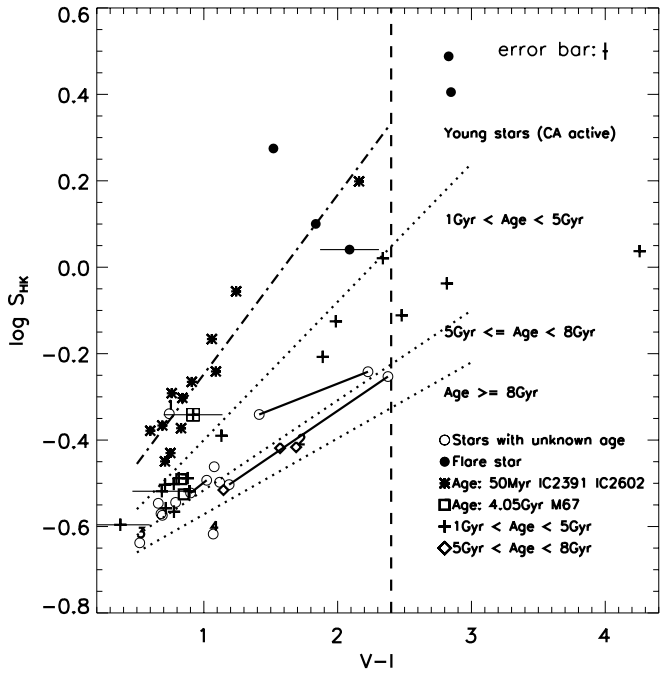

Figure 2. Relation among $\log(S_{\rm HK})$, $V-I$, and age. Open circles represent CPMB stars with an unknown age. Filled circles are flare stars. Stars in clusters IC2602 + IC2391 and M67 are shown as asterisks and squares, respectively. Plus signs and diamonds represent stars with different ages: 1 Gyr < age < 5 Gyr and 5 Gyr < age < 8 Gyr, respectively. Four domains are divided by dotted lines. The dash-dotted line is the least-squares fit of young clusters IC2602+IC2391. The vertical dashed line is $V-I=2.4$. To the right of this, CA is not expected to depend on age. Solid lines connect the MS components in CD-31 7352/LP902-30, LP684-1/2, and LP387-1/2. The star indicated as number 1 is G163-B9A. Numbers 2–3 denote halo star candidates (LHS300A and CD-31 1454). Number 4 is the star with the weakest activity in our sample (G114-B8B). The typical error bar for our measurement is in the upper right corner. Separate $V-I$ uncertainties are given for four stars whose $V-I$ were estimated by the relation in Figure 1. A square with a plus sign is an outlier (G95-B5A) that seems overactive for its age domain. This star is perhaps a close binary and it warrants follow-up observations to determine the cause of its high CA.

3.3. Discussion

All MS stars are plotted in Figure 2, which displays our empirical relation among $\log(S_{\rm HK})$, age, and $V-I$. Asterisks represent the young cluster stars in IC2602 and IC2391 that have the same age 50 ± 5 Myr (Barrado y Navascués et al. 2004). It is clear that $\log(S_{\rm HK})$ tends to be larger in red stars and smaller in blue stars at the same age. Two M67 cluster member stars are plotted with squares. M67 is much older than IC2602 and IC2391 and these points clearly demonstrate the expectation that CA declines with age. The plus signs represent field stars whose ages are between 1.0 Gyr and 5.0 Gyr. Diamonds represent stars whose ages are between 5.0 Gyr and 8.0 Gyr. Our sample includes five known flare stars (40 Eri C, LP891-13, LP888-63, G216-B14A, BD+26 730) which are displayed as filled circles. These clearly show enhanced CA for their supposed age.

Figure 2 can be divided into four arbitrary age domains, represented by dotted lines. The top domain mainly consists of young active stars and flare stars. The other three domains consist of less active stars whose ages are, respectively, 1.0–5.0 Gyr, 5.0–8.0 Gyr, and >8.0 Gyr. The typical uncertainty in $V-I$ and $\log(S_{\rm HK})$ for inactive stars is displayed at the right top of Figure 2 as an error bar. A least-squares fit to stars in IC2602 and IC2391 (dash-dotted line) illustrates that this group conforms to a consistent age in the $\log(S_{\rm HK})$ versus $V-I$ plane.

Stars to the right of the vertical dashed line at $V-I=2.4$ are later in spectral type than ∼dM3. Silvestri et al. (2005) found no Skumanich-style CA versus age relation among stars later than dM3, in accord with the expectation that a so-called "turbulent dynamo" drives CA in such stars (see Reid & Hawley 2000, and references therein). Thus, stars in this region are not expected to follow the CA versus age relation seen in earlier spectral type MS stars.

Overall, it can be seen that CA generally decays with age from 50 Myr to at least 8 Gyr for stars with $1.0 \leqslant V-I \leqslant 2.4$. However, for stars bluer than $V-I \approx 1.0$, CA shows little variation between 1.0 and 5.0 Gyr, which is consistent with the results of Pace et al. (2009) who found that CA from 1.4 Gyr (NGC3680) to 4.0 Gyr (M67) remains almost constant. Also note that lines of constant age do not have the same slope. For young stars, the lines of constant age have a relatively steep slope, while they appear to be much flatter for old stars.

Some comments on a few individual stars in Figure 2 are appropriate. The star labeled as 1 in Figure 2 is G163-B9A. Its companion, G163-B9B, was identified as an sdB star by Wegner & Reid (1991) and Catalán et al. (2008b). The CA of G163-B9A is very strong. Thus, it is either a very young star or perhaps was observed during a flare event. The latter possibility was eliminated based on a detailed examination of its spectrum. Thus, we conclude that G163-B9A/B is probably not a physical pair. Stars labeled as 2 and 3 are possible halo stars; star 4 has the weakest CA. These will be discussed in Section 5.

There are five wide binaries (CD-31 1454/LP888-25, G114-B8A/B, CD-31 7352/LP902-30, LP684-1/2, and LP387-1/2) that consist of pairs of MS stars. Only LP387-1/2 was observed at KPNO while all others were observed at CTIO. Since the two components of coeval binaries are expected to have consistent levels of CA, this provides a good reality check on our CA, $V-I$, and age relation. Unfortunately, the spectrum of LP888-25, the companion to CD-31 1454, was unusable because of low signal-to-noise ratio. In addition, we concluded that G114-B8A/B is not a physical binary because the components' radial velocities are inconsistent. The solid lines in Figure 2 connect the MS components in the other three pairs, CD-31 7352/LP902-30, LP684-1/2, and LP387-1/2, that most likely are physical pairs. The components in CD-31 7352/LP902-30 and LP387-1/2 have CA consistent with the same age. Some age difference is implied in LP684-1/2, though the difference is within the uncertainty implied by the error bar in the upper right corner of Figure 2. Clearly, CA, along with radial velocity, provides a very useful way for filtering out nonphysical pairs.

4. THE AGE–[Fe/H] RELATION

The metallicity of each MS star was estimated by comparing the observed spectra to a set of template spectra. Initially, a library of low-resolution theoretical spectra was generated using the SYNTH program, based on Kurucz's New Opacity Distribution Function atmospheric models (Castelli & Kurucz 2003). The atmosphere models assume local thermodynamic equilibrium. A mixing length of $l/H_{\rm p}=1.25$ and a microturbulence $\xi=2$ km s^{-1} were adopted. The line list included the atoms and molecules from Kurucz (1993). The maximum correlation method was applied to find the closest matching theoretical spectra to each observed spectrum. Since our objects are MS stars, we adopted $\log g=4.5$ and [Fe/H] = 0.0 as initial values. The effective $T_{\rm eff}$ was then estimated based on the maximum

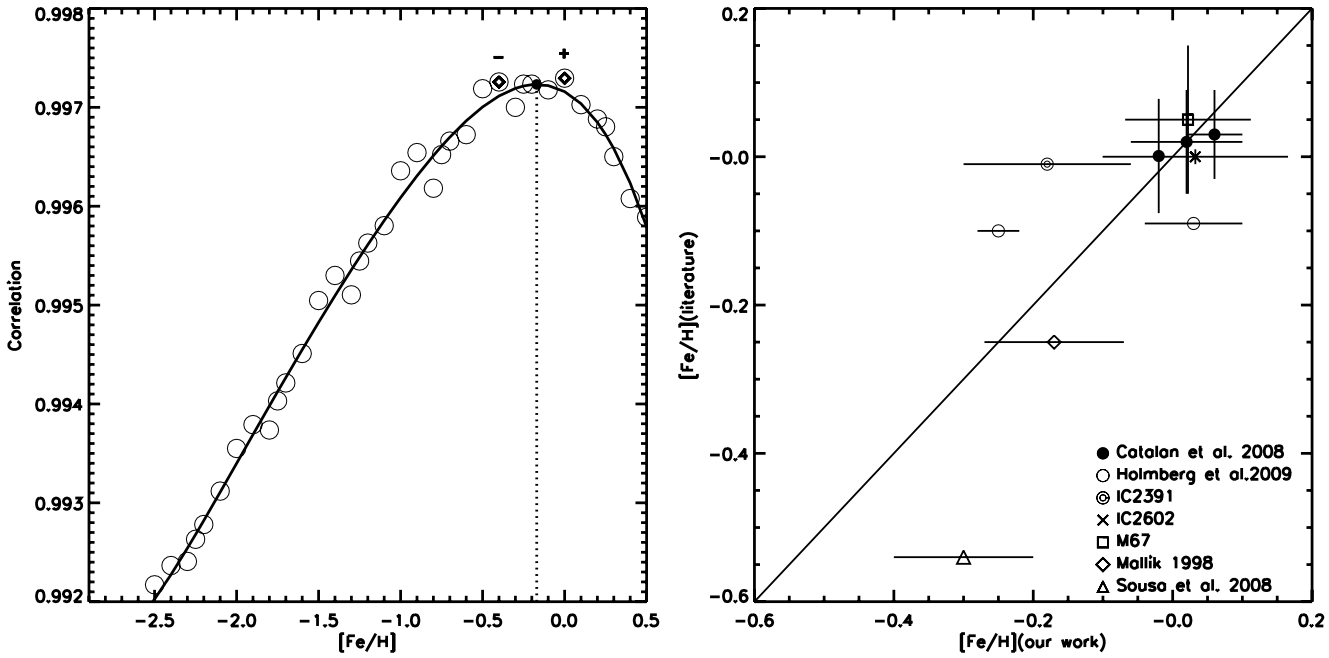

Figure 3. Left: an example of how [Fe/H] estimates were made with the maximum correlation method. The filled circle is the maximum of a fitted polynomial. The [Fe/H] correlated to this maximum is regarded as our final result. + and − signs indicate our estimate of uncertainty as discussed in the text. Right: the comparison between our [Fe/H] results and those in the literature. Filled circles represent stars in Catalán et al. (2008b). Single open circles represent stars in Holmberg et al. (2009). Double open circles, X signs, and squares represent the clusters IC2391, IC2602, and M67, respectively. We adopted the average [Fe/H] of member stars as the final cluster [Fe/H]. The [Fe/H] of IC2391 and IC2602 are from D'Orazi & Randich (2009), while that of M67 is from Pancino et al. (2010). Diamonds and triangles represent stars in Mallik (1998) and Sousa et al. (2008), respectively. Note that many of these sources did not give uncertainties, hence no vertical error bars could be plotted.

correlation method. Once an estimated $T_{\rm eff}$ was obtained, a new estimated [Fe/H] could be obtained with the same procedure. After several iterations, the best-fitting parameters stabilized and computations were terminated. The left panel of Figure 3 displays the correlation coefficient versus [Fe/H] in a typical fit. Each open circle represents one template. The filled circle is the maximum correlation coefficient obtained from polynomial fitting (solid line). The value of [Fe/H] at this point is regarded as our best estimate for this star's metallicity. The diamond points mark the templates yielding the maximum correlation ("+": the highest template point above; "−": the highest template point below). The difference in [Fe/H] between the two diamond points and the filled circle is taken as the estimated uncertainty in metallicity. The right panel of Figure 3 compares our [Fe/H] estimates to those which could be found in the literature. The mean difference is smaller than 0.15 dex, suggesting our metallicity is basically consistent with that of other work. [Fe/H] measurements were not made for stars later than M3 because we do not have templates for the latest spectra nor could we expect the CA versus age determination to be valid in such late-type MS stars. The resulting metallicities estimated for 37 MS stars in our sample are given in Column 10 of Table 3.

Although one of the key consequences of the stellar evolution theory is the gradual increase in the metal content of the interstellar medium and the progressive enrichment of subsequent stellar generations, some studies have found little, if any, indication that an age–metallicity relation (AMR) exists among solar neighborhood late-type stars. For example, Rocha-Pinto et al. (2000) studied the AMR using a sample of 552 late-type dwarfs. For those stars, metallicities were estimated from *uvby* data, and ages were calculated from their chromospheric emission levels using a metallicity-dependent CA versus age relation developed by Rocha-Pinto & Maciel (1998). The resulting AMR was found

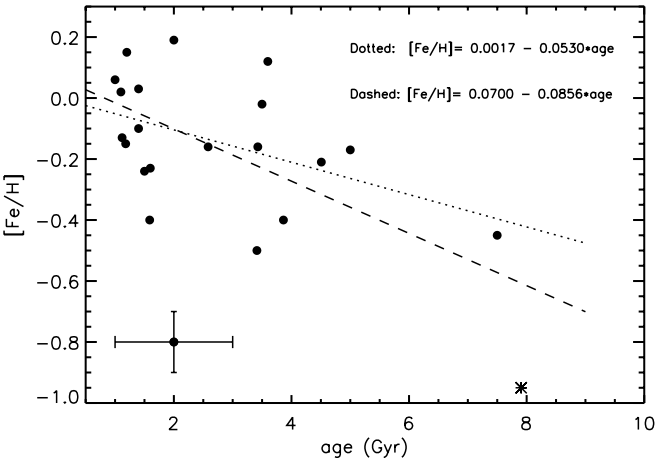

Figure 4. Our [Fe/H] vs. age relation for 21 MS stars. Typical uncertainties in age and [Fe/H] are displayed at the lower left of this figure. Filled circles represent disk stars. Only one star indicated by an asterisk (LHS300A) is a likely halo star. The dotted line is a least-squares fit for only disk stars, while the dashed line includes all stars.

to be a smooth function in their analysis. Feltzing et al. (2001) found that the solar neighborhood age–metallicity diagram is well populated at all ages in a sample of 5828 dwarf and subdwarf stars from the *Hipparcos* Catalog. Bensby et al. (2004) investigated the AMR using a sample of 229 nearby thick disk stars. Their results indicate that there is indeed an AMR in the thick disk. They found that the median age decreases by about 5–7 Gyr when going from [Fe/H] ≈ -0.8 to [Fe/H] ≈ -0.1.

Figure 4 is our [Fe/H] versus age relation for 21 stars. An asterisk represents one likely halo star (see the following section). Disk stars are displayed as filled circles. The typical

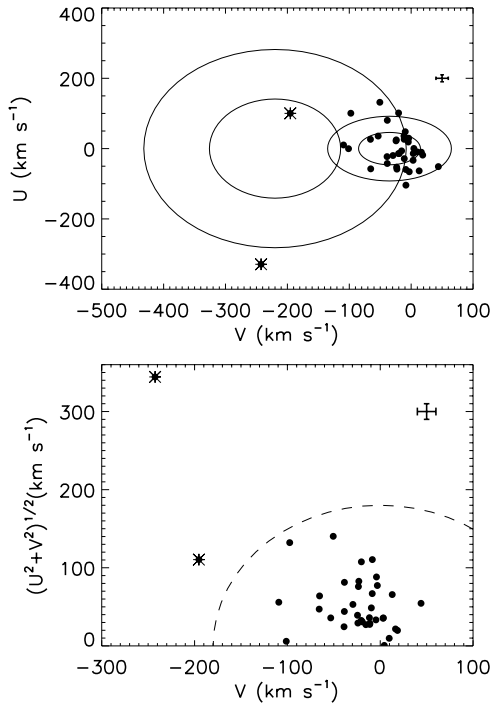

Figure 5. Top: *UV*-velocity distribution of our sample with measured v_r (km s^{-1}). The ellipsoids indicate the 1σ (inner) and 2σ (outer) contours for Galactic thick-disk and stellar halo populations, respectively. Typical error bars are given in both panels. Bottom: Toomre diagram of our stars. Dashed line is $V_{\rm total} = 180$ km s^{-1}.

uncertainties in age and [Fe/H] are shown at the left bottom of this figure. The dotted line is a least-squares fit for disk stars only, while the dashed line is the fit for all stars. The expected trend in age–metallicity is apparent: old stars tend to be of lower metallicity.

Our [Fe/H] versus age relation differs somewhat from the early work on single stars by Barry (1988, see Figure 5 in that reference). Our Figure 4 shows a more clear trend, quite similar in fact to the newer study of field stars by Rocha-Pinto et al. (2000); the slopes of their relation and ours are approximately the same. We conclude that wide binaries exhibit an [Fe/H]–age relation similar to field stars. However, at present our sample contains too few stars to support a detailed examination of the nearby star formation history.

5. POPULATION MEMBERSHIP

Column 6 of Table 3 lists the parallaxes of our wide binaries. Some trigonometric parallaxes were obtained from the Simbad Astronomical Database (Genova 2006). For 11 wide binaries lacking trigonometric parallaxes, we computed photometric parallaxes using Equations (3)–(5) which were derived from the data in Bergeron et al. (2001):

$$\pi = 10^{-(\frac{V-M_V+5}{5})} \quad (3)$$

$$M_v = 12.2199 + 1.8152(V-I) + 2.9704(V-I)^2 - 1.7082(V-I)^3 \quad (4)$$

$$M_v = 11.7099 + 6.6038(B-V) - 3.7273(B-V)^2 + 0.8066(B-V)^3. \quad (5)$$

The rectangular velocity components relative to the Sun for 41 MS stars were then computed and transformed into Galactic velocity components U, V, and W, and corrected for the peculiar solar motion $(U, V, W) = (-9, +12, +7)$ km s^{-1} (Wielen 1982). The *UVW*-velocity components are defined as a right-hand system with U being positive in the direction radially outward from the Galactic center, V being positive in the direction of Galactic rotation, and W being positive perpendicular to the plane of the Galaxy in the direction of the north Galactic pole. The typical uncertainties in U, V, and W are no more than $\sim$10 km s^{-1}. Columns 7–9 of Table 3 list our computed U, V, and W velocity components.

The top panel of Figure 5 shows contours, centered at $(U, V) = (0, -220)$ km s^{-1}, that represent 1σ and 2σ velocity ellipsoids for stars in the Galactic stellar halo as defined by Chiba & Beers (2000). Six stars lie outside the 2σ velocity contour centered on $(U, V) = (0, -35)$ km s^{-1} defined for disk stars (Chiba & Beers 2000). The bottom of Figure 5 shows the Toomre diagram of our stars. Venn et al. (2004) suggest stars with $V_{\rm total} > 180$ km s^{-1} are possible halo members. There

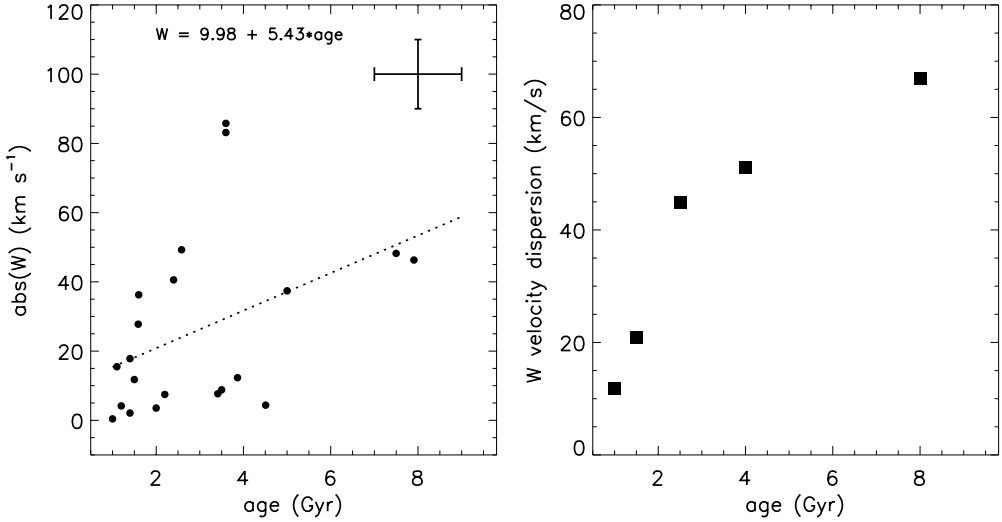

Figure 6. Left: age vs. absolute value of the W component of space velocity for 21 MS stars in our CPMB sample. Solid line is a least-squares fit. Typical uncertainties in age and W are displayed at the upper right of this figure. Right: W dispersion vs. age derived by binning the data in the left panel in five age groups ranging from 1–8 Gyr.

are two stars that meet this criterion. Taking metallicity, space motion, and CA into account, they have a high probability of belonging to the halo population. One is LHS300A ([Fe/H] = -0.95 ± 0.25) which is identified as a thick disk star in Monteiro et al. (2006). Considering the metallicity and space motion, we think it is a halo star. The other is CD-31 1454 ([Fe/H] = -0.48 ± 0.02) which is regarded as a halo star by Chanamé & Gould (2004). The two likely halo stars are also labeled in Figure 2 as numbers 2 and 3, respectively. Their CA is weak, suggesting ages in excess of 5 Gyr. These two plausible halo stars are displayed as asterisks plus filled circles in the bottom panel of Figure 5. The star numbered 4 in Figure 2 is G114-B8B ([Fe/H] = -0.40 ± 0.08) which may be the oldest star in our sample. Its age appears to be older than 8 Gyr as suggested by its location in Figure 2. The other stars are most likely members of the disk. The above analysis demonstrates the difficulty of making a population assignment on the basis of only space velocity or metallicity or CA. Ideally all three should be used.

The left panel of Figure 6 displays the computed absolute value of the W components of our stars' space motions versus estimated ages for 21 stars for which complete information is available. As expected, old stars tend to have larger W velocity. A weak positive correlation between the vertical velocity (W) of stars in CPMBs and age is expected based on the standard paradigm for stellar encounters in the disk. The right panel of Figure 6 presents the dispersion in W as a function of age. It is clear that in general the W dispersion becomes larger with age from 1 Gyr to 8 Gyr.

6. CONCLUSION

In this study we presented the CA levels, ages, metallicities, and space motions for components of 36 wide binaries. WD components were identified in 31 wide binaries. We also observed a sample of cluster member stars with well-determined ages in order to test the expected CA versus age relation. The ages of 23 wide binaries were derived by the cooling time of each WD companion added to the lifetime estimate of its progenitor.

We first examined the relation among log ($S_{\rm HK}$), $V - I$, and age. Our results support the expected hypothesis established among single and cluster MS stars, i.e., in general CA declines with age for stars with $1.0 \leqslant V - I \leqslant 2.4$ from 50 Myr to at least 8 Gyr. However, for stars with $V - I < 1.0$, the CA varies little between 1 Gyr and 5 Gyr. This is consistent with results of Pace et al. (2009) who found nearly constant CA level from 1.4 Gyr (NGC3680) to 4.0 Gyr (M67). Apparently the slope in the log($S_{\rm HK}$) versus $V - I$ plane for young stars is relatively steep, while for old stars it appears to be flatter. Additional observations will be required to determine whether this slope changes monotonically or discontinuously with age. These limitations will need to be taken carefully into account by anyone attempting to use CA to determine ages for single stars.

The metallicities of stars earlier in spectral type than M3 were measured by template matching. Our sample generally supports the expected paradigm, i.e., older stars tend to have lower metallicity. However, it also underscores the fact that there is much variation in metallicity at all ages, precluding its use for determining ages for single stars. Also, the AMR among wide binaries appears to be quite comparable to that found in single field stars (Rocha-Pinto et al. 2000).

With trigonometric parallaxes from the literature and photometric parallaxes derived from B, V, R, I data, proper motions, and our measured v_r values, we calculated full space motions U, V, and W for as many of our MS stars as possible. Our results clearly show that the W dispersion increases with age. In general, the W velocity component is also relatively larger for old stars. Using our measurements of CA and metallicity, we concluded that two wide binaries (CD-31 1454/LP888-25 and LHS300A/B) are probably halo members, while the others are disk stars. This low fraction of halo members among wide binaries is consistent with the earlier results of Silvestri et al. (2002) who found only one halo binary in their sample of WD+dM pairs. We estimated that the oldest disk star in our sample is G114-B8B (>8 Gyr) based on its weak CA.

Five of our wide binaries consist of two MS stars. Two (G114-B8A/B and G163-B9A/B) apparently are not physical pairs, since the two companions have inconsistent CA levels, radial velocities, and/or metallicities. CD-31 7352/LP902-30 and LP387-1/2 are physical pairs because the two MS components have very similar velocities, metallicity, and CA level. LP684-1/2 is probably a physical pair since the radial velocity difference between two components is within the range of uncertainty and its components display a comparable $S_{\rm HK}$ value.

In conclusion, our study affirms the assumption that wide binaries (CPMBs) share the same kinematic and spectroscopic properties as nearby single field and cluster stars. Thus, they are very promising resources for studying stellar populations and age groups that are not well sampled by nearby clusters.

T.D.O. acknowledges support from NSF grant AST-0807919 to Florida Institute of Technology. J.K.Z., G.Z., and Y.Q.C. acknowledge support from NSFC grant Nos. 10821061, 11073026, and 11078019. We are also grateful for constructive comments by the reviewer that substantially improved our paper.

REFERENCES

Baliunas, S. L., et al. 1995, ApJ, 438, 269
Barnes, S. A. 2007, ApJ, 669, 1167
Barnes, S. A., Sofia, S., & Prosser, C. F. 1999, ApJ, 516, 265
Barrado y Navascués, D., Stauffer, J. R., & Jayawardhana, R. 2004, ApJ, 614, 386
Barry, D. C. 1988, ApJ, 334, 436
Barry, D. C., Cromwell, R. H., & Hege, E. K. 1987, ApJ, 315, 264
Bennett, C. L., et al. 2003, ApJS, 148, 97
Bensby, T., Feltzing, S., & Lundström, I. 2004, A&A, 421, 969
Bergeron, P., Leggett, S. K., & Ruiz, M. T. 2001, ApJS, 133, 413
Bergeron, P., Saffer, R. A., & Liebert, J. 1992, ApJ, 394, 228
Bergeron, P., Wesemael, F., Lamontagne, R., Fontaine, G., Saffer, R. A., & Allard, N. F. 1995, ApJ, 449, 258
Bochanski, J. J., West, A. A., Hawley, S. L., & Covey, K. R. 2007, AJ, 133, 531
Castelli, F., & Kurucz, R. L. 2003, in IAU Symp. 210, Modelling of Stellar Atmospheres, Poster Contributions, ed. N. Piskunov, W. W. Weiss, & D. F. Gray (San Francisco, CA: ASP), A20
Catalán, S., Isern, J., García-Berro, E., & Ribas, I. 2008a, MNRAS, 387, 1693
Catalán, S., Isern, J., García-Berro, E., Ribas, I., Allende Prieto, C., & Bonanos, A. Z. 2008b, A&A, 477, 213
Chanamé, J., & Gould, A. 2004, ApJ, 601, 289
Chaussidon, M. 2007, in Lectures in Astrobiology II, ed. M. Gargaud, H. Martin, & P. Claeys (Berlin: Springer), 45
Chiba, M., & Beers, T. C. 2000, AJ, 119, 2843
D'Orazi, V., & Randich, S. 2009, A&A, 501, 553
Feltzing, S., Holmberg, J., & Hurley, J. R. 2001, A&A, 377, 911
Fontaine, G., Brassard, P., & Bergeron, P. 2001, PASP, 113, 409
Genova, F. 2006, Centre de Données astronomiques de Strasbourg, http://simbad.u-strasbg.fr/
Giampapa, M. S., Hall, G. C., Radick, R. R., & Baliunas, S. L. 2006, ApJ, 651, 444
Giclas, H. L., Burnham, R., & Thomas, N. G. 1971, Lowell Proper Motion Survey, Northern Hemisphere: The G Numbered Stars (Flagstaff, AZ: Lowell Observatory)

Gray, R. O., Corbally, C. J., Garrison, R. F., Mcfadden, M. T., & Robinson, P. E. 2003, AJ, 126, 2048
Greenstein, J. L. 1986, AJ, 92, 859
Hall, J. C., Lockwood, G. W., & Skiff, B. A. 2007, AJ, 133, 862
Holmberg, J., Nordström, B., & Andersen, J. 2009, A&A, 501, 941
Iben, I., & Laughlin, G. 1989, ApJ, 341, 312
Jorgensen, B. R., & Lindegren, L. 2005, A&A, 436, 127
Koester, D., Voss, B., Napiwotzki, R., Christlieb, N., Homeier, D., Lisker, T., Reimers, D., & Heber, U. 2009, A&A, 505, 441
Koester, D., et al. 2001, A&A, 378, 556
Kurucz, R. L. 1993, Kurucz CD-ROM 13, ATLAS9 Stellar Atmosphere Programs and 2 km/s Grid (Cambridge, MA: SAO)
Luyten, W. J. 1979, Proper Motion Survey with the 48 Inch Telescope (Minneapolis, MN: Univ. Minnesota Press)
Mallik, S. V. 1998, A&A, 338, 623
Mamajek, E. E., & Hillenbrand, L. A. 2008, ApJ, 687, 1264
Monteiro, H., Jao, W. C., Henry, T., Subasavage, J., & Beaulieu, T. 2006, ApJ, 638, 446
Noyes, R. W., Hartmann, L. W., Baliunas, S. L., Duncan, D. K., & Vaughan, A. H. 1984, ApJ, 279, 763
Oswalt, T. D., Hintzen, P. M., & Luyten, W. J. 1988, ApJS, 66, 3910
Oswalt, T. D., Sion, E. M., Hintzen, P. M., & Liebert, J. W. 1991, in NATO ASI Ser. C 336, White Dwarfs, ed. G. Vauclair & E. M. Sion (Dordrecht: Kluwer), 379
Oswalt, T. D., Smith, J. A., Shufelt, S., Hintzen, P. M., Leggett, S. K., Liebert, J., & Sion, E. M. 1993, in NATO ASI Ser. C 403, White Dwarfs: Advances in Observation and Theory, ed. M. A. Barstow (Dordrecht: Kluwer), 419
Pace, G., Melendez, J., Pasquini, L., Carraro, G., Danziger, J., François, P., Matteucci, F., & Santos, N. C. 2009, A&A, 499, L9
Pace, G., & Pasquini, L. 2004, A&A, 426, 1021
Pancino, E., Carrera, R., Rossetti, E., & Gallart, C. 2010, A&A, 511, 56
Patten, B. M., & Simon, T. 1993, ApJ, 415, L123
Patten, B. M., & Simon, T. 1996, ApJS, 106, 489
Reid, N. I., & Hawley, S. L. 2000, New Light on Dark Stars: Red dwarfs, Low-Mass Stars, Brown Dwarfs (London: Springer)
Rocha-Pinto, H. J., & Maciel, W. J. 1998, MNRAS, 298, 332
Rocha-Pinto, H. J., Maciel, W. J., Scalo, J., & Flynn, C. 2000, A&A, 358, 850
Silvestri, N. M., Hawley, S. L., & Oswalt, T. D. 2005, AJ, 129, 2428
Silvestri, N. M., Oswalt, T. D., & Hawley, S. L. 2002, AJ, 124, 1118
Silvestri, N. M., et al. 2006, AJ, 131, 1674
Sion, E. M., Holberg, J. B., Oswalt, T. D., McCook, G. P., & Wasatonic, R. 2009, AJ, 138, 1681
Skumanich, A. 1972, ApJ, 171, 565
Smith, J. A. 1997, PhD thesis, Florida Institute of Technology
Soderblom, D. R. 2010, ARA&A, 48, 581
Soderblom, D. R., Duncan, D. K., & Johnson, D. H. R. 1991, ApJ, 375, 722
Sousa, S. G., et al. 2008, A&A, 487, 373
Valenti, J. A., & Fischer, D. A. 2005, ApJS, 159, 141
Vaughan, A. H., & Preston, G. W. 1980, PASP, 92, 385
Venn, K. A., Irwin, M., Shetrone, M. D., Tout, C. A., Hill, V., & Tolstoy, E. 2004, AJ, 128, 1177
Voss, B., Koester, D., Napiwotzki, R., Christlieb, N., & Reimers, D. 2007, A&A, 470, 1079
Wegner, G., & Reid, I. N. 1991, ApJ, 375, 674
Weidemann, V. 2000, A&A, 363, 647
Weidemann, V., & Koester, D. 1984, A&A, 132, 195
West, A. A., Hawley, S. L., Bochanski, J. J., Covey, K. R., Reid, I. N., Dhital, S., Hilton, E. J., & Masuda, M. 2008, AJ, 135, 785
Wielen, R. 1982, Landolt-Börnstein Tables, Astrophysics, Vol. 2C, Sec. 8.4 (Berlin: Springer), 202
Wilson, O. C. 1963, ApJ, 138, 832
Wilson, O. C. 1968, ApJ, 153, 221
Wood, M. 1995, in White Dwarfs, Vol. 443, ed. D. Koester & K. Werner (Berlin: Springer), 41